ICAS 2020 SHANG HAI
International Council of the Aeronautical Sciences
32nd Congress of the International Council of the Aeronautical Sciences
September 6-10, 2021
Pudong Shangri-La, Shanghai, China

Effects of adverse pressure gradient on the behaviours of resolvent mode

Cheng Chen[1,2], Jiang-tao Huang[1] & Xian Chen[1]

[1]Air-breathing Hypersonic Technology Research Center, China Aerodynamics Research and Development Center, No.6 Erhuannan Road, Mianyang 621000, China
[2]State Key Laboratory of Aerodynamics, China Aerodynamics Research and Development Center, No.6 Erhuannan Road, Mianyang 621000, China

Abstract

With the purpose of investigating the effects of adverse pressure gradient on the coherent structures of turbulent boundary layer, we have carried out the resolvent analysis, proposed by Professor McKeon at Caltech, of both pure Couette flow corresponding to ZPG (flow case C, γ is the ratio of wall shear at the moving wall to that at the stationary wall τ_M^* / τ_S^* and is equal to 1) and a shear-less flow with APG producing nearly zero mean shear at the moving wall (flow case SL, $\gamma \approx 0$), which is somewhat similar to the case of APG TBL at the verge of separation and has relatively detailed DNS database. The results show that the APG applied for flow case SL leads to a small decrease in singular value (i.e. the amplification rate of resolvent mode). Specifically, this APG yields a 6% decrease in gain (i.e. the ratio of SL to C singular value is $\sigma_{\mathbf{k},SL} / \sigma_{\mathbf{k},C} = 0.94$). Under the premise that the two cases have near-identical forcing strengths for this mode as a result of almost the same mean shear near the stationary wall, which plays a primary role in the mechanisms of turbulence production, this observation is consistent with the statement on inner/outer layer interactions in turbulent CP flows by Pirozzoli *et al.*, who found that the coherent streaky structure near the stationary wall is suppressed in terms of velocity fluctuations in the cross-stream components and concluded that the imprinting and amplitude modulation imparted by large-scale events in the channel core onto the near-wall motions increase gradually from flow case P to case SL to case C. Furthermore, it is also found that APG leads to the disappearance of the symmetry of the streamwise energy density distribution and its redistribution and the large coherent energetic structure is seen to be squeezed towards the upper wall by APG.

Keywords: adverse pressure gradient; turbulent boundary layers; coherent structure; resolvent mode; amplification rate

1. Introduction

A better understanding of the behaviours of wall-bounded turbulent flows, relevant to many fluid-flow systems of technological interest such as the flow over aircraft wings and wind turbine blades or in compressors, has been a benchmark problem in turbulence research community and received considerable attention in the last two decades. Notwithstanding several ideal scenarios with zero pressure gradient (ZPG) for these systems, e.g. turbulent Couette flow[1-2] and ZPG turbulent boundary layer (TBL) [3-4], has been studied to explore essential aspects of wall-bounded turbulence widely, it is acknowledged that ZPG condition is rarely encountered in practical applications and the majority of flow problems are featured by the complexity of pressure gradient. In particular, adverse pressure gradient (APG) existing in relation with convex curved surfaces may produce flow separation and result in consequent performance losses, such as the lift decrease and drag increase of airfoil. As it has been confirmed that the extension of the knowledge from ZPG wall-bounded turbulence to APG cases, which are less dealt with, is relatively limited[5] and

the depiction of their many aspects of the scaling, structure and stability remains unsatisfactory, it is necessary to investigate the behaviours of APG wall-bounded turbulence more deeply with emphasis on the effect mechanisms of the imposed pressure gradient.

Since McKeon[6] introduced the concept of resolvent analysis in the context of turbulent pipe flows, it has become an efficient tool for analyzing the turbulent flow behaviours which are featured by the energy transfer from the mean flow to all the velocity scales and the intrinsical linear amplification as well as nonlinear redistribution mechanisms[7]. The low-rank nature of transfer function H_k, which appears as or related to the resolvent of state operator in the sub-system of linearized NSE, is proved to enable the significant simplification of model formulation and implementation of flow control scheme[8-9]. Considering the works by McKeon and co-authors on resolvent analysis, there are three distinct research layers. The first one, accomplished mainly by McKeon & Sharma, is with regard to the resolvent analysis tool itself. They raised the basic idea of using resolvent analysis for understanding the physics of wall-bounded turbulence[6,10], presented the exemplary operations of response mode superposition to recreate complex coherent structures and clarified the correspondence relationship between Koopman mode decomposition, resolvent mode decomposition and exact invariant solutions of NSE[11]. The second involves the rank-1 model subject to broadband forcing, which is used to illuminate various scaling relationships and geometric self-similarity in turbulent pipe and channel flows. The last one, conducted primarily by Luhar et al., is centered on the investigation of control effects of wall blowing/suction and compliant surface, which could induce skin friction reduction and suppression of energetic structures in wall turbulence effectively[8].

In this paper, we identify the effects of APG on wall-bounded turbulence by accessing the resolvent modes obtained via resolvent analysis, which are confirmed to represent turbulent flow structures and account for the effects of control availably. With a significantly simpler mean flow and boundary condition, fully developed turbulent Couette-Poiseuille (CP) flows are chosen as the subject of ongoing research. The main flow parameters for such flows are the friction Reynolds number $\mathrm{Re}_{\tau S} = u_{\tau S}^* h^* / \nu^*$ (the superscript * denotes a dimensional quantity), which is defined based on the friction velocity at the stationary wall $u_{\tau S}^*$, the channel half-width h^* and kinematic viscosity ν^*, and the ratio of wall shear at the moving wall to that at the stationary wall $\gamma = \tau_M^* / \tau_S^*$. Our focus is on two cases of turbulent CP flow with different values of γ: pure Couette flow corresponding to ZPG (flow case C, $\gamma \approx 1$) and a shear-less flow with APG producing nearly zero mean shear at the moving wall (flow case SL, $\gamma \approx 0$), which is somewhat similar to the case of APG TBL at the verge of separation and has relatively detailed DNS database. The relative difference between these two cases in the structure and amplification of the resolvent modes is used to infer the effects of APG.

2. Approach

2.1 Resolvent analysis

The turbulent CP flow of an incompressible Newtonian fluid considered is governed by the continuity equation and NSE, i.e.

$$\nabla \bullet \mathbf{u} = 0, \tag{1}$$

$$\frac{\partial \mathbf{u}}{\partial t} = -\nabla p - \mathbf{u} \bullet \nabla \mathbf{u} + \frac{1}{\mathrm{Re}_{\tau S}} \Delta \mathbf{u}, \tag{2}$$

where ∇ and $\Delta = \nabla \bullet \nabla$ are the gradient operator and the Laplacian respectively, $\mathbf{u}(x, y, z, t)$ and

$p(x, y, z, t)$ denote the velocity vector and pressure, and t is the time. The streamwise (x) and spanwise (z) directions are both infinitely long, and the normal direction is finite with $-1 \le y \le 1$; see figure 1 for the geometry. The velocities, spatial variables, time and pressure are normalized by $u_{\tau S}^*$, h^*, $h^* / u_{\tau S}^*$ and $\rho^* u_{\tau S}^{*2}$ respectively, where ρ^* is the density. When normalized by the viscous length scale $\nu^* / u_{\tau S}^*$, the spatial variables are represented with a superscript '+' following standard notation.

With the introduction of the Fourier transform in the homogeneous directions x, z and time t, the velocity field is decomposed as

$$\mathbf{u}(x, y, z, t) = \iiint \mathbf{u}_{\mathbf{k}}(y; k_x, k_z, \omega) e^{i(k_x x + k_z z - \omega t)} dk_x dk_z d\omega, \tag{3}$$

where $\mathbf{u}_{\mathbf{k}}(y; k_x, k_z, \omega)$ represents a propagating wave with streamwise and spanwise wavelengths $\lambda_x = 2\pi / k_x$ and $\lambda_z = 2\pi / k_z$ and with a streamwise speed $c = \omega / k_x$ for any wavenumber-propagating speed combination $\mathbf{k} = (k_x, k_z, c) \neq 0$.

The mean velocity profile $\mathbf{U}(y) = [U(y)\ 0\ 0]^T$ corresponds to $\mathbf{k} = (0, 0, 0)$. We use a high-resolution DNS code, applied to SS-HST[12], to determine $U(y)$. In detail, the values of streamwise velocity from DNS are averaged in both streamwise and spanwise directions, where periodicity is enforced for the rectangular box of computational domain, and then the time average is further performed with the data samples at sufficiently large t, considering the statistically stationary nature of the simulations.

By treating the convective nonlinearity in (2) as a forcing term $\mathbf{f} = -\mathbf{u}\bullet\nabla\mathbf{u}$ and substituting (3) into (1) as well as (2), the following linear forcing-response system is obtained for velocity fluctuations $\mathbf{u}_{\mathbf{k}}$ and pressure fluctuation $p_{\mathbf{k}}$:

$$\begin{aligned} \begin{bmatrix} \mathbf{u}_{\mathbf{k}} \\ p_{\mathbf{k}} \end{bmatrix} &= \left(-i\omega \begin{bmatrix} \mathbf{I} & 0 \\ 0 & 0 \end{bmatrix} - \begin{bmatrix} \mathbf{L}_{\mathbf{k}} & -\nabla_{\mathbf{k}} \\ \nabla_{\mathbf{k}}^T & 0 \end{bmatrix} \right)^{-1} \begin{bmatrix} \mathbf{I} \\ 0 \end{bmatrix} \mathbf{f}_{\mathbf{k}} \\ &= \mathbf{H}_{\mathbf{k}} \mathbf{f}_{\mathbf{k}}, \end{aligned} \tag{4}$$

where $\nabla_{\mathbf{k}} = [ik_x, \partial_y, ik_z]^T$ and $\nabla_{\mathbf{k}}^T$ denote the gradient and divergence operators in spectral space, and $\mathbf{f}_{\mathbf{k}} = (-\mathbf{u}\bullet\nabla\mathbf{u})_{\mathbf{k}}$ is the nonlinear forcing term projected in the wavenumber-propagating speed direction $\mathbf{k}$. The linear operator $\mathbf{L}_{\mathbf{k}}$ contained in the resolvent $\mathbf{H}_{\mathbf{k}}$, which provides substantial information about the input-output relationship between the forcing and the velocity and pressure response, is written as

$$\mathbf{L}_{\mathbf{k}} = \begin{bmatrix} -ik_x U + \mathrm{Re}_{\tau S}^{-1} \nabla_{\mathbf{k}}^2 & -\partial U / \partial y & 0 \\ 0 & -ik_x U + \mathrm{Re}_{\tau S}^{-1} \nabla_{\mathbf{k}}^2 & 0 \\ 0 & 0 & -ik_x U + \mathrm{Re}_{\tau S}^{-1} \nabla_{\mathbf{k}}^2 \end{bmatrix}, \tag{5}$$

where $\nabla_{\mathbf{k}}^2 = -k_x^2 + \partial^2 / \partial y^2 - k_z^2$ is the Fourier-transformed Laplacian.

Following McKeon & Sharma[6] and Luhar *et al.* [8], an SVD of $\mathbf{H}_{\mathbf{k}}$ is performed to yield a series of orthonormal forcing ($\mathbf{f}_{\mathbf{k},m}$) and response ($[\mathbf{u}_{\mathbf{k},m},\ p_{\mathbf{k},m}]^T$) modes, which are ranked in an energetic sense

$$\mathbf{H}_{\mathbf{k}} = \sum_m \psi_{\mathbf{k},m} \sigma_{\mathbf{k},m} \phi_{\mathbf{k},m}^*,\ \sigma_{\mathbf{k},1} > \sigma_{\mathbf{k},2} > \ldots > \sigma_{\mathbf{k},m} > \ldots > 0. \tag{6}$$

The resolvent operator is proved to be of low rank and the model based solely on the first response mode ($\mathbf{u}_{\mathbf{k},1}$ and $p_{\mathbf{k},1}$), i.e. the rank-1 approximation, can reproduce some experimental or DNS observations reasonably, under the premise of neglecting the nonlinear interaction between resolvent modes. Thus, the present paper employs it for the study of the effects of APG on turbulent CP flows. For the remainder of this paper, the additional subscript '1' is dropped and the term 'resolvent modes' only refers to the rank-1 velocity and pressure fields. Moreover, for this chosen model with broadband forcing, we define the premultiplied streamwise energy density of the principal response of resolvent operator by

$$E_{uu}(y;\mathbf{k}) = k_x^2 k_z \sigma_{\mathbf{k}}^2 (|u|(y;\mathbf{k}))^2, \tag{7}$$

such that the one-dimensional density dependent on c and the intensity for streamwise velocity are derived by integrating $E_{uu}(y;\mathbf{k})$ over the corresponding wave parameter spaces J as

$$E_{uu}(y,c) = \iint_J E_{uu}(y;\mathbf{k}) d\log(k_x) d\log(k_z), \tag{8}$$

$$E_{uu}(y) = \iiint_J E_{uu}(y;\mathbf{k}) d\log(k_x) d\log(k_z) dc, \tag{9}$$

and the other one-dimensional densities (e.g. $E_{uu}(y,k_x)$ and $E_{uu}(y,k_z)$) can be determined similarly.

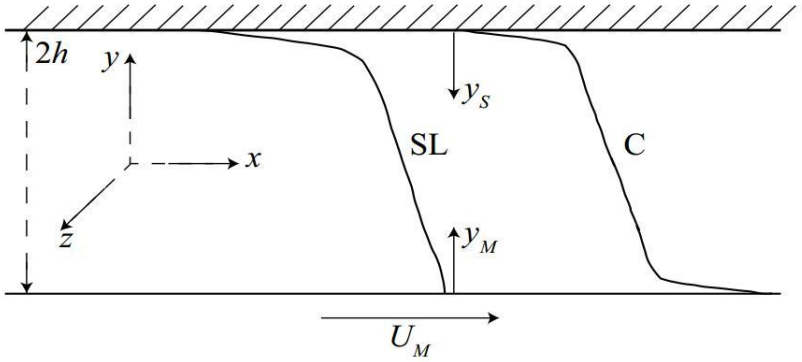

Figure 1 – Sketch of mean velocity profiles for flow case C and SL. y_S and y_M are the wall normal distances from the stationary wall and the moving wall, respectively. U_M=U(y=-1) denotes the mean velocity at the moving wall.

2.2 Numerical implementation

The resolvent operator in (4) is discretized in the normal direction using a spectral collocation method on Chebyshev points. The differentiation matrices are computed by means of the MATLAB differentiation matrix suite developed by Weideman & Reddy[13]. Unlike turbulent channel flow[7], the mean flow profile of turbulent CP flow is not characterized by symmetry across the centreline (e.g. flow case SL), and the pairing of structurally similar response modes with near-identical singular values is invisible. Hence, the imposition of symmetry by the modification of differentiation matrices is herein abandoned and Chebyshev points are used for the discretization in the whole channel domain $-1 \le y \le 1$ with a larger value of N_y relative to that in Ref. [7].

The SVD of discretized resolvent operator is performed by Matlab's svds algorithm for each wavenumber-propagating speed combination. Considering the three-dimensional wave parameter space that needs to be explored and the large size of discretized resolvent operator (four times the number of collocation points in y), its parallel implementation is enabled based on the utilisation of

multi-cores, especially for the derivation of energy densities and intensities.

3. Results and discussions

With the convenience of resolvent formulation to evaluate the effects of APG over spectral space, this section concentrates on two classes of modes resembling the near-wall coherent structure (NW cycle) and the very-large-scale motions (VLSMs) firstly, which are shown to be dynamically important in many previous studies on turbulent Couette flow. For the former, we consider the wavenumber-propagating speed combination $\mathbf{k} = (k_x, k_z, c) = (2.54, 17.77, 10.35)$ at $\mathrm{Re}_{\tau S} = 282$ corresponding to wavelengths $\lambda_x^+ = 700$ and $\lambda_z^+ = 100$, which are indicated by the peak positions of the pre-multiplied energy spectra for the near-wall region. While for the latter, the combination $\mathbf{k} = (k_x, k_z, c) = (0.13, 1.40, 18.72)$ is investigated at $\mathrm{Re}_{\tau S} = 282$ corresponding to wavelengths $\lambda_x = 50$ and $\lambda_z = 4.5$, which are chosen to be the medial values in the ranges of streamwise and spanwise length scales for VLSMs in the core region[2,14].

Thereafter, the results on both resolvent modes are followed by discussions concerning the effects of APG on the streamwise energy spectra (3.3).

3.1 Near-wall modes

The velocity field for flow case C associated with the NW-type resolvent mode is shown in figure 2. Consistent with known features of the NW cycle, the velocity field in the spanwise-wall normal plane ($x = 0$) shows counter-rotating quasi-streamwise vortices localized just above the critical layer $y_{cS} = 0.053$ ($y_{cS}^+ = 15$), where the mode speed matches the local mean velocity. The velocity vector field in the streamwise-wall normal plane ($z = 0$) presents alternating prograde and retrograde rotation. Further, the regions of maximum (minimum) wall pressure are coincident with those of increasing (decreasing) wall-normal velocity, implying that the wall-pressure field may have a phase difference approximately equal to π/2 with wall-normal velocity field.

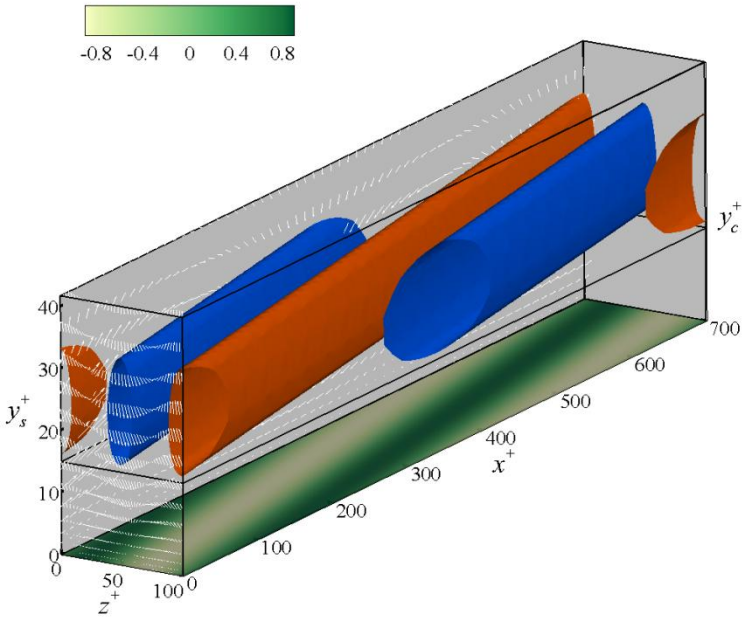

Figure 2 – Velocity structure for the NW-type mode $\mathbf{k} = (k_x, k_z, c) = (2.54, 17.77, 10.35)$ at $\mathrm{Re}_{\tau S} = 282$ for case C. The red-and-blue isosurfaces show positive and negative wall-normal velocities at 80% of maximum absolute value. The shading at the stationary wall represents the normalized wall-pressure field.

The structure of this mode is exhibited in figure 3(a-c) in terms of the amplitude, phase and Reynolds stress profiles. The streamwise velocity and pressure field peaks at the critical layer while the wall-normal velocity peaks at a location farther from the stationary wall. The phase difference between the streamwise velocity and wall-normal velocity is about 0 at the critical layer and thus the Reynolds stress contribution also peaks near y_c (figure 3c), which are proved to be typical characteristics for high-gain resolvent modes. Further, the wall-normal velocity has a near-constant $\pi/2$ phase difference with pressure field, similar to the null cases in turbulent Poiseuille flow, as the main source of pressure field is likewise the fast source term in the Poisson equation, although the sign of phase difference is reversed due to the transformation of coordinate system (from y to y_S).

The APG applied for flow case SL leads to a small decrease in singular value. Specifically, this APG yields a 6% decrease in gain (i.e. the ratio of SL to C singular value is $\sigma_{\mathbf{k},SL} \,/\, \sigma_{\mathbf{k},C} = 0.94$). Under the premise that the two cases have near-identical forcing strengths for this mode as a result of almost the same mean shear near the stationary wall, which plays a primary role in the mechanisms of turbulence production, this observation is consistent with the statement on inner/outer layer interactions in turbulent CP flows by Pirozzoli *et al.*[15], who found that the coherent streaky structure near the stationary wall is suppressed in terms of velocity fluctuations in the cross-stream components and concluded that the imprinting and amplitude modulation imparted by large-scale events in the channel core onto the near-wall motions increase gradually from flow case P to case SL to case C. As shown in figure 3(d-f), this decrease is not accompanied by a significant change in mode structure. The streamwise velocity as well as the pressure contribution peaks near the critical layer similarly and the wall-normal velocity peaks at a location slightly farther from the stationary wall. The major distinction is that the locations of the peak values of streamwise and wall-normal velocities as well as pressure are all shifted towards the stationary wall slightly together with the critical layer, where the streamwise velocity and wall-normal velocity are still 0 out of phase. Thus the Reynolds stress contribution for flow case SL also peaks near y^+_{cS} (figure 3f). Further, for identical forcing strengths, the 6% decrease in mode amplitude would lead to a near-11% decrease of the absolute value of the actual Reynolds stress generated by this mode.

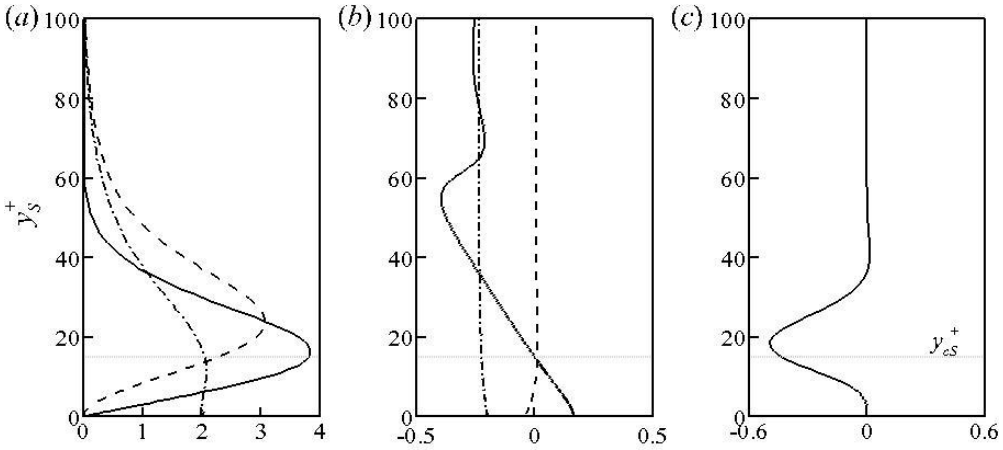

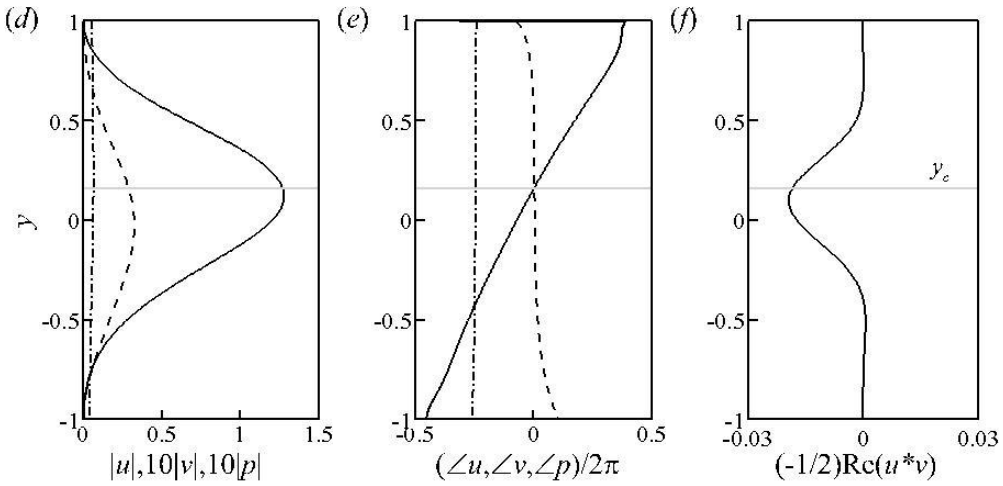

Figure 3 – Profiles showing the wall-normal variation in (a,d) amplitude and (b,e) phase for the streamwise velocity (solid lines), wall-normal velocity (dashed lines) and pressure (dash dot lines) for the resolvent modes resembling the NW cycle. (c,f) The normalized Reynolds stress contribution. Panels (a-c) represent flow case C and (d-f) represent flow case SL.

3.2 Very-large-scale motions

Unlike the scenario of turbulent Poiseuille flow[8], figure 4(a-c) shows that the flow case C structure for the VLSM resolvent mode with over 10-fold increase in wavelength is quite different from that for the NW mode considered in the previous section. The peak values of streamwise velocity, wall-normal velocity and Reynolds stress are now located at or near the channel center y=0, where the critical layer lies, and they have a larger wall-normal extent relative to their counterparts for the NW mode. With the increase of mode speed c, the flow structure associated with this mode detaches from the stationary wall entirely with decreased magnitude of the wall-pressure field, which results from the weaker source terms in the pressure Poisson equation (the mean velocity gradient is smaller close to the channel center). Nevertheless, similar to the NW mode, there is also a near-constant $\pi/2$ phase difference between $v_{\mathbf{k}}$ and $p_{\mathbf{k}}$ and the phase difference between the streamwise velocity and wall-normal velocity is about 0 at the critical layer.

Different from the mode resembling the NW cycle, the VLSM mode is amplified by the APG imposed with a 23% increase in gain (i.e. the ratio of SL to C singular value is $\sigma_{\mathbf{k},SL} / \sigma_{\mathbf{k},C} = 1.23$). Note that this fact is not in conflict with the DNS observation that velocity fluctuations in the three components are all suppressed by APG at the channel core, as the production term P relevant to forcing strength for flow case C is apparently larger than that for case SL[15]. The mode structure with APG imposed is modified such that the location of the peak value of streamwise velocity is shifted towards the stationary wall slightly together with the critical layer, while the magnitude of the wall-normal velocity still exhibits local maxima near the channel core. The streamwise velocity and wall-normal velocity are still 0 out of phase at the critical layer, producing thereby the peak value of Reynolds stress contribution.

The flow case C structure associated with this large-scale mode is similar to that shown in figure 2 (not shown here), but with vastly different length scales. Flow case SL has a smaller magnitude of pressure field at the moving wall relative to flow case C, as the latter has stronger source term in the pressure Poisson equation and thus a larger wall-pressure signature there.

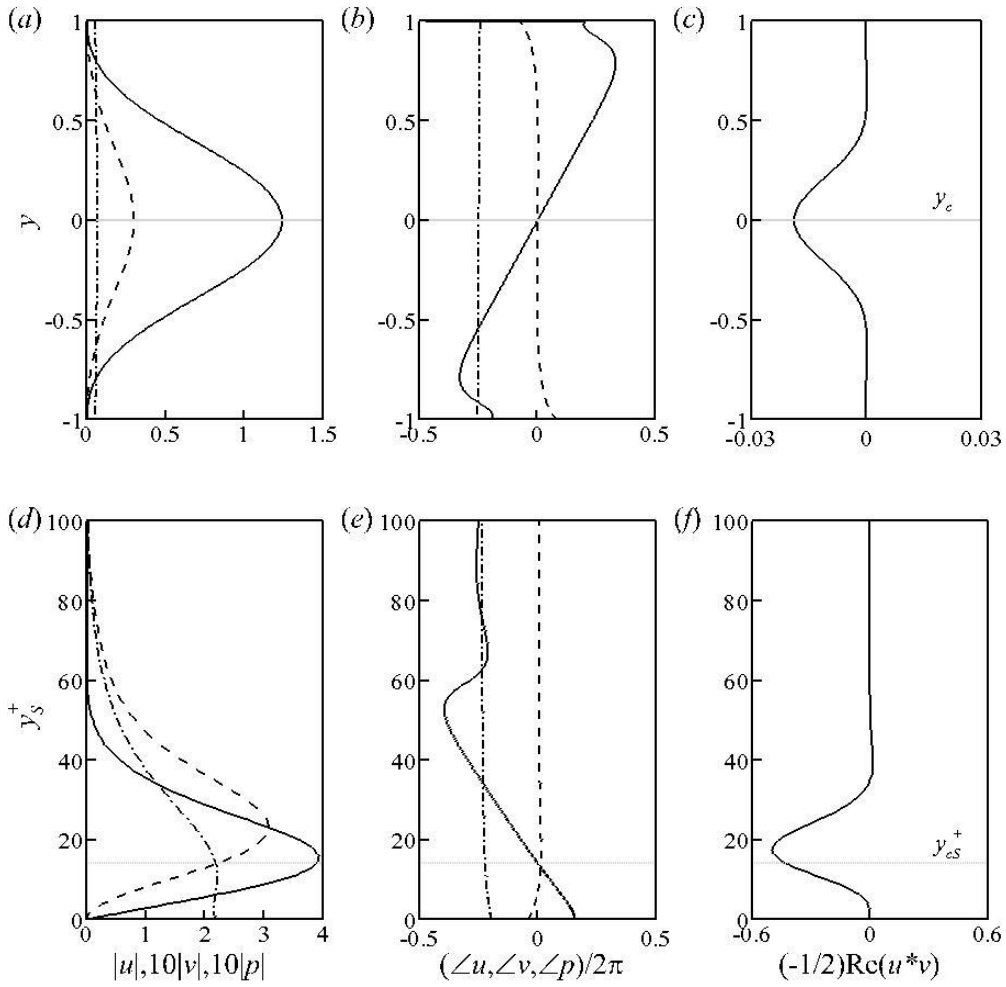

Figure 4 – Profiles showing the wall-normal variation in (a,d) amplitude and (b,e) phase for the streamwise velocity (solid lines), wall-normal velocity (dashed lines) and pressure (dot dash lines) for the resolvent modes resembling the VLSMs. (c,f) The normalized Reynolds stress contribution. Panels (a-c) represent flow case C and (d-f) represent flow case SL.

3.3 Effect of APG on the streamwise energy spectra

In this section, we compare the resolvent-based prediction for pre-multiplied streamwise energy spectra, which yields immediate understanding of the energetic relevance of the various scales of motions, with that from previous DNS studies to verify the efficiency of rank-1 approximation to capture the characteristics of the most energetic modes of real turbulent channels and to reveal further the effect of APG on the turbulent energy spectra.

The square roots of energy intensities for streamwise, wall-normal and spanwise velocity fluctations as well as the Reynolds shear stress are reported in figure 5, which permits a direct comparison with root-mean-square (r.m.s.) velocity fluctuation for varying value of γ. APG is seen to have minor influence in close proximity of the stationary wall, where the flow is dominated by the local shear. Further, the velocity fluctuations in the upper half of the channel are not apparently strongly affected by APG, even near the channel centerline, where significant differences are found for all the Reynolds stress components in the DNS study of Pirozzoli *et al*. Oppositely, the velocity fluctuations in the lower half of the channel are obviously suppressed by APG. The near-wall peak of streamwise velocity fluctuation vanishes in flow case SL, implying that the wall cycle mechanism of turbulence regeneration does not exist herein.

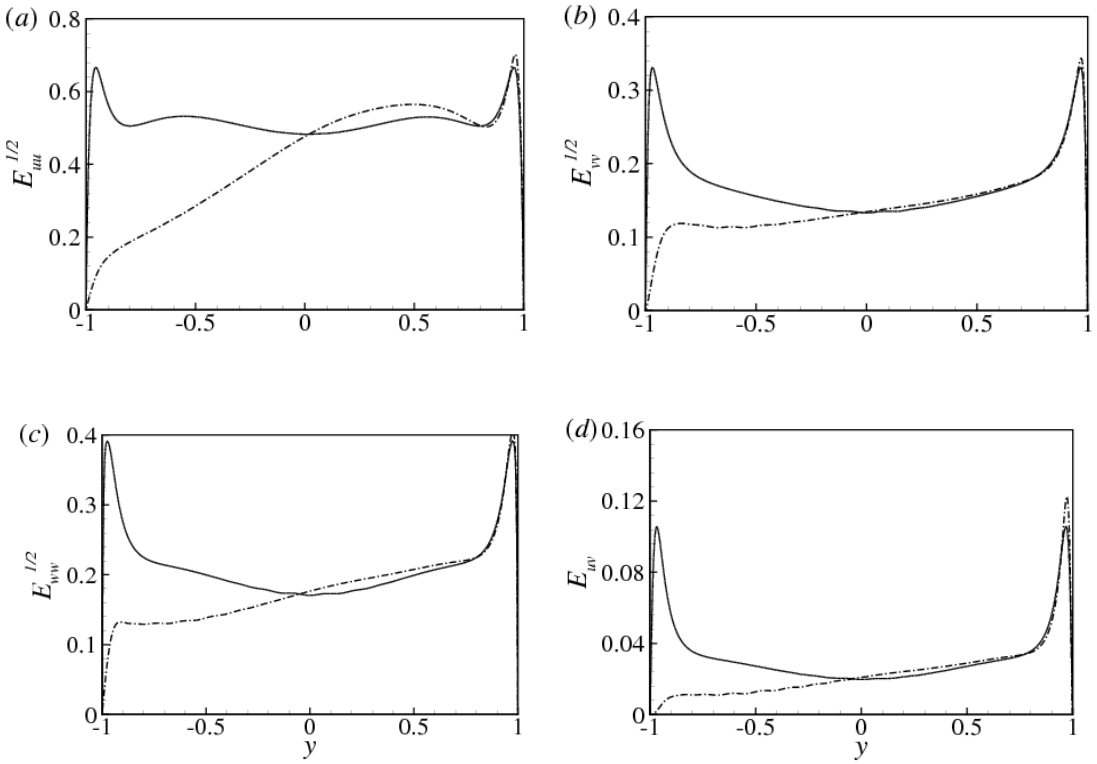

Figure 5 – The distributions of the energy intensities for streamwise, wall-normal and spanwise velocity fluctuations as well as the Reynolds shear stress across the channel. The dotted line denotes flow case C and the dash dot line represents flow case SL.

As shown in figure 6, two distinct peaks, specular with respect to the centerline, are observed in the spanwise power spectral density for flow case C, and their energies are concentrated about $\lambda_z \approx 0.20$ (corresponding to $\lambda_z^+ \approx 56$). These peaks are located at a distance from the wall y_S, $y_M \approx 0.045$ (corresponding to $y^+ \approx 13$) and correspond to the typical signature of the regeneration cycle of near-wall turbulence, although quantitative differences are found for the spanwise wavelength λ_z^+ and wall-normal location y^+. Consistent with the DNS result with moderate Reynolds number and a large computational box, an obvious secondary peak is observed near the channel centerline with $\lambda_z \approx 2.5$, associated with possible VLSM, and the length scale of energetic motion seems to increase steadily as the channel centerline is approached. The ridge departing from this secondary peak and extending to the vicinity of both walls may be seen as a sign of imprinting mechanism of the outer motions on the near-wall ones. When APG is imposed (flow case SL), the depletion of energy in the proximity of the lower wall is observed and a low-wavenumber energy maximum forms in the upper part of the channel, whose energy is concentrated about $\lambda_z \approx 0.16$ and $y_S \approx 0.038$ (corresponding to $y^+ \approx 11$) and which is structurally similar with the near-wall peaks observed in flow case C. Note that the trend that the wall-normal location of near-wall peak is shifted towards the stationary wall by APG is consistent with the result of resolvent analysis for the NW mode (figure 3). Further, an obvious secondary peak is observed further away from the upper wall about $\lambda_z \approx 2$, very similar to that reported in Pirozzoli *et al.*[15].

A similar organization of the power spectral density is also observed in the streamwise spectra $k_x E_{uu}$ (figure 7). The large-scale motion, centered in the core of the channel in flow case C, has a faint signature in the streamwise spectra and its streamwise length is $\lambda_x \approx 20$ based on the interpretation of the locations of the weak spectral peaks. Note that this length from the streamwise spectra is less than that from DNS observation, as the meandering feature of the streaks[16] and the

assumption of identical forcing strengths lead to the uncertainty of the prediction for actual geometry feature of large-scale motion. While for flow case SL, the break of symmetry and the depletion of energy in the proximity of the lower wall are again observed in (y, λ_x) plane with the secondary peak having a larger length of $\lambda_x \approx 30$.

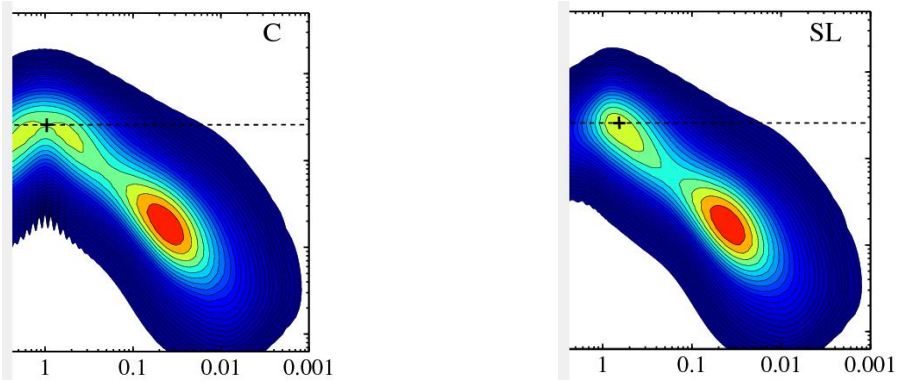

Figure 6 – Pre-multiplied streamwise energy spectra in the spanwise direction ($k_z E_{uu}$) at various wall-normal locations. The distance from the nearest wall (y_S, y_M) is reported on the horizontal axis in logarithmic scale to emphasize the near-wall behaviour. 26 logarithmically spaced contour levels from 1% of the maximum value to the maximum value are shown. The black crosses denote the peak locations of the spectral densities for $\lambda_z = 2.5$.

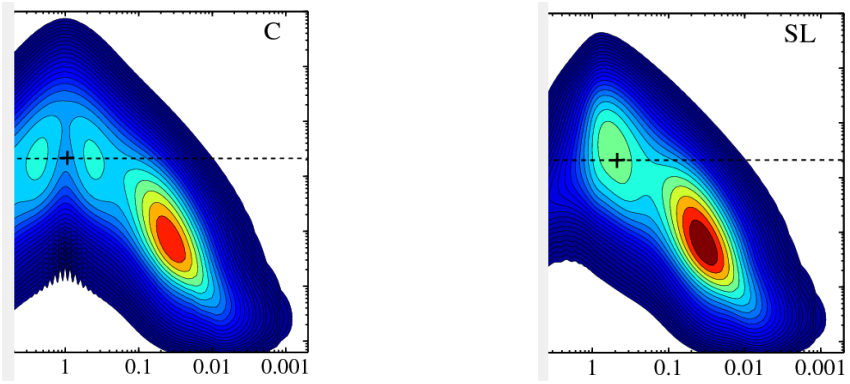

Figure 7 –Pre-multiplied streamwise energy spectra in the streamwise direction ($k_x E_{uu}$) at various wall-normal locations. The distance from the nearest wall (y_S, y_M) is reported on the horizontal axis in logarithmic scale to emphasize the near-wall behaviour. 26 logarithmically spaced contour levels from 1% of the maximum value to the maximum value are shown. The black crosses denote the peak locations of the spectral densities for $\lambda_x = 20$.

4. Conclusions

In this paper, we use the methodology to investigate the effects of APG on the amplification factor and shape of resolvent mode. The results show that for NW mode, the APG applied for flow case SL leads to a 6% decrease in gain (i.e. the ratio of SL to C singular value is $\sigma_{\mathbf{k},SL} / \sigma_{\mathbf{k},C} = 0.94$), and this decrease is not accompanied by a significant change in mode structure. The VLSM mode is amplified by the APG imposed with a 23% increase in gain (i.e. the ratio of SL to C singular value is $\sigma_{\mathbf{k},SL} / \sigma_{\mathbf{k},C} = 1.23$), different from the mode resembling the NW cycle. The mode structure with APG imposed is modified such that the location of the peak value of streamwise velocity is shifted towards the stationary wall slightly together with the critical layer, while the magnitude of the wall-normal velocity still exhibits local maxima near the channel core.

Furthermore, it is also found that APG leads to the disappearance of the symmetry of the streamwise energy density distribution and its redistribution, and the large coherent energetic

structure is seen to be squeezed towards the upper wall by APG.

5. Copyright Statement

References

[1] Bech K H, Tillmark N, Alfredsson P H and Andersson H I. An investigation of turbulent plane Couette flow at low Reynolds numbers. *J. Fluid Mech.*, 286, pp 291–325, 1995.

[2] Avsarkisov V, Hoyas S, Oberlack M and Garcia-Galache J P. Turbulent plane Couette flow at moderately high Reynolds number. *J. Fluid Mech.,* 751, R1, 2014.

[3] Perry A E and Li J D. Experimental support for the attached-eddy hypothesis in zero-pressure-gradient turbulent boundary layers. *J. Fluid Mech.,* 218, pp 405–438, 1990.

[4] Smits A J, McKeon B J and Marusic I. High-Reynolds number wall turbulence. *Annu. Rev. Fluid Mech.,* 43, pp 353–375, 2011.

[5] Monty J P, Harun Z and Marusic I. A parametric study of adverse pressure gradient turbulent boundary layers. *Int. J. Heat Fluid Fl.,* 32, pp 575–585, 2011.

[6] McKeon B J and Sharma A S. A critical-layer framework for turbulent pipe flow. *J. Fluid Mech.,* 658, pp 336–382, 2010.

[7] Moarref R, Sharma A S, Tropp J A and McKeon B J. Model-based scaling of the streamwise energy density in high-Reynolds-number turbulent channels. *J. Fluid Mech.,* 734, pp 275–316, 2013.

[8] Luhar M, Sharma A S and McKeon B J. A framework for studying the effect of compliant surfaces on wall turbulence. *J. Fluid Mech.*, 768, pp 415–441, 2015.

[9] Gómez F, Blackburn H M, Rudman M, Sharma A S and McKeon B J. A reduced-order model of three-dimensional unsteady flow in a cavity based on the resolvent operator. J. Fluid Mech., 798, R2, 2016.

[10] Sharma A S and McKeon B J. Perturbation energy production in pipe flow over a range of Reynolds numbers using resolvent analysis. 47th AIAA Aerospace Sciences Meeting, Orlando, pp 1513, 2009.

[11] Sharma A S, Moarref R, McKeon B J, Park J S, Graham M D and Willis A P. Low-dimensional representations of exact coherent states of the Navier-Stokes equations from the resolvent model of wall turbulence. Phys. Rev. E, 93, 021102, 2016.

[12] Sekimoto A, Dong S W and Jiménez J. Direct numerical simulation of statistically stationary and homogeneous shear turbulence and its relation to other shear flows. Phys. Fluids, 28, 035101, 2016.

[13] Weideman J. A. C and Reddy S C. A MATLAB differentiation matrix suite. ACM Trans. Math. Softw., 26, pp 465–519, 2000.

[14] Rawat S, Cossu C, Hwang Y and Rincon F. On the self-sustained nature of large-scale motions in turbulent Couette flow. J. Fluid Mech., 782, pp 515–540, 2015.

[15] Pirozzoli S, Bernardini M and Orlandi P. Large-scale motions and inner/outer layer interactions in turbulent Couette-Poiseuille flows. J. Fluid Mech., 680, pp 534–563, 2011.

[16] Hutchins N and Marusic I. Large-scale influences in near-wall turbulence. Phil. Trans. R. Soc. Lond. A, 365, pp 647–664, 2007.